Contents lists available at ScienceDirect

Food and Bioproducts Processing

journal homepage: www.elsevier.com/locate/fbp

Development of a 'millimanipulation' device to study the removal of soft solid fouling layers from solid substrates and its application to cooked lard deposits

Akin Ali[a,*], *Dominic de'Ath*[a], *Douglas Gibson*[a], *Jennifer Parkin*[a], *Zayeed Alam*[b], *Glenn Ward*[b], *D. Ian Wilson*[a]

[a] *Department of Chemical Engineering and Biotechnology, New Museums Site, Pembroke Street, Cambridge CB2 3RA, United Kingdom*

[b] *Proctor & Gamble Technical Centres Ltd., Whitley Road, Longbenton, Newcastle-upon-Tyne NE12 9TS, UK*

ABSTRACT

A mm-scale scraping device was developed to study the removal behaviour of soft solid fouling layers (thickness 0.5–10 mm) from solid substrates. A blade is dragged through the circular or rectangular samples at controlled speed and the resistance forces measured. Tests with a viscous liquid (honey) and viscoplastic material (a Vaseline®-carbon black paste) indicated that cohesive deformation dominated the measured force. Two model food soils were: (i) unbaked lard and (ii) lard baked for different times with and without added ovalbumin. The cohesive strength of the baked lard, and its removal behaviour, changed noticeably following autoxidative polymerisation. Ovalbumin delayed the onset of polymerisation.

Keywords: Adhesion; Cohesive strength; Cleaning; Fouling; Fats; Rheology

1. Introduction

The formation of fouling layers from baked fats and oils is a widespread problem in food processing, causing equipment degradation, unhygienic conditions and, on household appliances, an undesirable appearance. Food fats and oils are mixtures of mono, di- and tri-glycerides as well as other hydrophobic components. During frying and baking, proteins and starches can be added to the melt. Fouling deposits are formed by oxidative polymerisation of the unsaturated components to give solid or semi-solid layers, which can adhere strongly to the process surfaces. Extended (or repeated) heat treatment promotes further polymerisation, colour changes and ultimately, at higher temperatures, degradation to carbonaceous (coke) layers.

These layers are amongst the most challenging to remove and cleaning often requires strong chemical treatments and/or large mechanical forces. Both of these can lead to degradation of the underlying substrate and an increase in surface roughness (i.e. scratches), which can increase the propensity for further fouling and microbial growth. Cleaning baked-on fat soils often involves a combination of chemical and mechanical actions, wherein a chemical reagent promotes softening of the soil layer so that it can be removed by fluid shear, impacting liquid jets or mechanical friction. Being able to measure the forces involved, and thereby the rheology and evolution of microstructure, of these materials during cleaning is highly desirable for understanding cleaning mechanisms and developing cleaning agents. As stiff semi-solid materials, these soils do not lend themselves to study by

* *Corresponding author*. Tel.: +44 7833 466 898.
E-mail address: aa620@cam.ac.uk (A. Ali).
Received 2 May 2014; Received in revised form 31 August 2014; Accepted 2 September 2014
Available online 22 October 2014
http://dx.doi.org/10.1016/j.fbp.2014.09.001

Nomenclature

Roman

a	Carreau–Yasudo model parameter, –
f	measured force, N
f_{I}	force component to displace material ahead of the blade, N
f_{II}	force component to raise displaced material, N
f_{III}	force component to resist material underneath blade, N
F_w	force per unit width, N m^{-1}
$F_{w,0}$	force per unit width at r/R = 0, N m^{-1}
F_w^0	plastic component of F_w, N m^{-1}
F_w^{I}	force per unit width to displace material ahead of the blade, N m^{-1}
F_w^{II}	force per unit width to raise displaced material, N m^{-1}
F_w^{III}	force per unit width to resist material under the blade, N m^{-1}
$\overline{F_w}$	average force per unit width, N m^{-1}
g	acceleration due to gravity, m^{-2}
G'	elastic modulus, Pa
G''	viscous modulus, Pa
L	blade thickness, m
m	Carreau–Yasudo power-law index, –
r	distance from sample center and millimanipulation tool, m
R	sample radius, m
R^2_{fit}	coefficient of determination, –
s	scrape depth, m
t	time, s
t_o	scraping time, s
V	scrape speed, m s^{-1}
V_{displace}	sample velocity at the substrate, m s^{-1}
$V_{\mathrm{substrate}}$	sample velocity at the substrate, m s^{-1}
w	width of the blade in contact with sample, m
w_t	width of the millimanipulation blade, m
x	distance scraped through sample relative to the point of first contact, m
y	co-ordinate, –

Greek

δ	clearance underneath millimanipulation blade, m
δ_o	initial thickness of soil, m
$\dot{\gamma}$	shear rate, s^{-1}
η	apparent viscosity, Pa s
η_0	viscosity at 0 shear rate, Pa s
η_∞	viscosity at infinite shear rate, Pa s
λ	characteristic viscoelastic time, s
τ_w	wall shear stress, Pa

Acronyms

BHT	butylated hydroxytoluene
DSC	differential scanning calorimetry
FT-IR	Fourier transform infrared spectroscopy
GPC	gel permeation chromatography
SS	stainless steel
Vas	Vaseline®
VCB	Vaseline® black paste

existing hydrodynamic devices such as the parallel plate flow cell (Bakker et al., 2003), impinging jet (Bayoudh et al., 2005), radial flow cell (Detry et al., 2007), rotating disc (Garca et al., 1997), the plynometer (Zorita et al., 2010) and fluid dynamic gauging (Chew et al., 2004). These all require the user to observe the moment and nature of removal at a length scale of several microns and above.

At smaller length scales, atomic force microscopy has been used to characterise adhesion and cohesion of foodstuffs such as caramel, sweetened condensed milk and Turkish delight (Akhtar et al., 2010) and biofilms (Garrett et al., 2008). Of the techniques mentioned, however, none provide a direct measure of the forces within a soil or the strength of attachment to the fouled surface. With the exception of the plynometer, they all generally require large liquid volumes and/or are time intensive. We present the commissioning of a device that is easy to use, requires little or no cleaning liquid and can make measurements quickly (≤5 min).

1.1. *From micro- to milli-manipulation*

Zhang and co-workers developed the micromanipulation technique at the University of Birmingham for studying the deformation of cells (Zhang et al., 1991) and their mechanical properties (Zhang et al., 1992; Yap et al., 2006). A modified 'micromanipulation' device was developed by Zhang and Fryer (Liu et al., 2002) to study the adhesive and cohesive forces within soiling layers. With this device, a horizontal bar (30 × 6 × 1 mm) is moved through the material at a set height from the substrate and the force on the bar measured. It is a controlled *strain* (or deformation) test, whereas the hydrodynamic devices mentioned above employ controlled (or estimated) *shear stress* conditions. By adjusting the level at which the tool is pulled through the layer, the technique can investigate cohesive (soil–soil) or adhesive (soil–substrate) interactions. Table 1 summarises studies where micromanipulation has been used to study foodstuffs, including proteinaceous (Liu et al., 2006a) and starch layers (Liu et al., 2006b). These studies have shown how sample rheology and soil–substrate interfacial properties affect both the strength of attachment and the type of removal observed.

The heterogeneity and the high cohesive strength of food fat soils prompted our development of a 'millimanipulation' tool designed to measure larger forces and work with deep layers, of thickness 0.2–10 mm. Baked fat layers, for example, have greater strengths than the material reported in Table 1. The strength of layers in the aforementioned studies ranges from ~0.3 to 80 J m^{-2} (as defined below). The millimanipulation device presented here, is shown to work on materials with a wider range of strength, including honey (~0.4 J m^{-2}) and baked lard (~420 J m^{-2}).

The schematic in Fig. 1(a) illustrates the working action: a vertical stainless steel blade is moved horizontally through the layer at velocity V. The layer is scraped from initial depth, δ_o, to final depth, δ. The force required to impose the strain is measured and video microscopes are used to record the deformation behaviour. The force measured, f, includes components required to (see Fig. 1):

(I) *Deform* material in the layer of thickness s, ahead of the blade, f_{I};
(II) *Displace* the deformed material, usually upwards along the face of the blade, f_{II};

Table 1 – Investigation of food soil deposits by modified micromanipulation technique. Significant figures are those reported in the original paper.

Soil	Substrate	Deposit thickness (mm)	Apparent cohesive strength ($J\,m^{-2}$)	Apparent adhesive strength ($J\,m^{-2}$)	Experimental variables investigated	Comments	Source
Tomato paste	316L SS	0.7–1.7	> 4	1–14	Hydration time, temperature and surface roughness	Samples weaken during hydration	Liu et al. (2002)
Whey protein	316L SS	1.5–2.8	0–10	0–10	Cleaning time and temperature	Increasing temperature and NaOH concentration (0.1–5 wt%)	Liu et al. (2006a)
Bread dough	316L SS	2.0	5–80	5–60	Air exposure time	Samples harden during exposure to air	Liu et al. (2006b)
Tomato paste	Ni-P-PTFE composites	1.2–3.6	2 –15	0.7 – 2.1	Effect of baking, substrate surface energy, sample thickness	Minimum sample adhesion occurs on surfaces with surface energies from 20 to 25 $mJ\,m^{-2}$	Liu et al. (2006b)
Corn oil	SS	3.2–1.7	<4	<4	Baking time and substrate	A layer of corn oil between substrate and deposit reduces adhesion	Liu et al. (2006)
Ovalbumin	316L SS	2.2	1.5–4	0.5–3	Cleaning time and temperature	Higher baking temperatures increase adhesive strength	Liu et al. (2007)

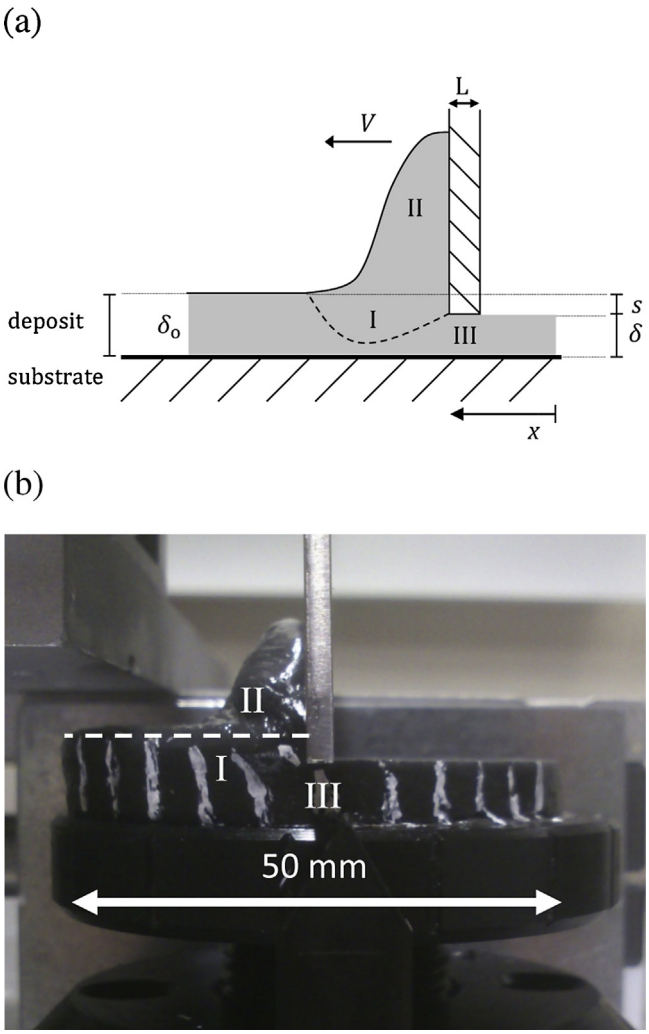

Fig. 1 – (a) Schematic of millimanipulation testing. A flat blade of thickness *L* is pulled at velocity, *V*, through a soil sample of initial thickness, δ_o, at a scrape depth, *s*, leaving a residual layer of notional thickness δ. The blade displacement, relative to the point of first contact is *x*. Region (I) denotes material ahead of the blade (boundary, dashed, not known *a priori*); (II) displaced material collected in front of the blade; and (III) material beneath the blade. (b) Photograph of Vaseline®-carbon black paste during millimanipulation testing. Vertical white lines of marker fluid were added to the sample for monitoring deformation.

(III) Overcome the *shear* resistance imposed on the bottom edge of the blade, f_{III};

such that:

$$f = f_I + f_{II} + f_{III} \quad (1)$$

The width of the blade in contact with the sample, w, can vary with displacement, e.g. for circular samples prepared on discs, so the force is reported as the force per unit width, F_w, viz.

$$F_w = f/w \quad (2)$$

which has units of $N\,m^{-1}$ (surface tension) or $J\,m^{-2}$ (surface energy). F_w can also be expressed in terms of the 3 components referred to above, giving:

$$F_w = F_w^I + F_w^{II} + F_w^{III} \quad (3)$$

For purely adhesive removal, i.e. δ close to 0; and $f_{II} = f_{III} = 0$, f can be compared with the adhesive work. It is noted that setting the blade along the surface, i.e. $\delta = 0$, is likely to invite contributions from surface friction. For the soils studied here, the cohesive strength, f_I is non-zero. The schematic in Fig. 1(a) pertains to cohesive removal of a viscous liquid or semi-solid soil. Fig. 1(b) shows an example of a Vaseline® carbon black (VCB) paste billet undergoing testing. If the removed soil does not adhere to the blade, f_{II} is negligible. The force transducer only measures forces in the horizontal plane; any shear caused by material climbing up the blade is not measured directly but the work required to elevate such material is reflected in F_w.

2. Materials and methods

2.1. Device

The millimanipulation device was designed to work with soil samples prepared on circular metal discs of diameter 50 mm. The unit was built around a force transducer (Sauter GmbH, FH5) with a measurement limit of 5000 mN and resolution ±1 mN. The transducer is mounted on a steel x–y table driven by two stepper motors allowing independent motion in the x and y directions at speeds ranging from 0.5 to 20 mm s^{-1}. The force is measured at a sampling rate of 20 Hz. The stepper motors are controlled via a desktop PC and data are logged using a LabVIEW™ application. The deformation is recorded by a video microscope (400X USB Microscope, Maplin Gadgets).

Two sample shapes were used for the studies reported here. Softer samples, such as honey, Vaseline® and lard, were prepared on circular discs. The tooth width, w_t, was selected to be wider than the sample, such that the length in contact with the blade, w, varies with scrape distance, x (see Fig. 2(a)). For harder layers, such as baked lard, a narrow rectangular section is prepared, such that w stays constant during scraping (see Fig. 2(b)). The tool is held vertical by lubricated guide rails (see Fig. 2(c) and (d)) connected to the force transducer and is pulled horizontally through the sample at constant speed, typically for 38 mm.

2.2. Sample preparation

Commissioning tests were conducted using honey (Sainsbury's Basic™, a viscous liquid), Vaseline® (a viscoplastic soft solid) and lard (a model food soil). Honey samples were prepared by pipetting 14 g of material on to 50 mm diameter (1 mm thick) stainless steel (SS) 316 test discs at room temperature. This procedure was found to give reproducible layers approximately 3.5 mm thick, measured using the video microscope.

Vaseline® and lard samples were spread evenly across 50 mm diameter discs with a spatula, using sets of half-ring formers to provide samples of known thickness (≤0.9 mm). As Vaseline® is translucent, samples were mixed with 5 wt% graphite powder (Fisher Scientific, UK) to give a VCB paste suitable for observation with the video microscope.

Model food fat layers were prepared using lard (Sainsbury's Basic™), baked for 1–5 h at temperatures of 50–250 °C. The melting point range of the lard, as measured by differential scanning calorimetry (DSC, data not presented here), was 27–38 °C. Lard was heated to 39 °C and egg white protein (ovalbumin: Sigma–Aldrich, grade II) was added to give a liquid mixture with protein contents ranging from 0 to 9.5 wt%. Aliquots of the mixture were pipetted on to the centre of a SS disc and allowed to spread out. The discs were placed in an oven for baking in air at the required temperature and duration. Samples were allowed to cool to room temperature before testing.

This method of preparation was suitable for preparing layers up to 200 μm thick. Some of these thin layers were, however, so hard that the forces required to remove them exceeded the instrument limit, or caused the blade to deflect. Thicker and somewhat softer samples were then prepared using SS discs with 0.6 mm high raised edges. The lard was loaded on to the disc and cooked as above. Rectangular samples, 12 mm wide and approximately 40 mm long, were created when the sample had cooled and by clearing the outer material away using a stencil and spatula (see Fig. 2(c) feature D). The tooth tool was used in these tests. The raised edge restricted the blade movement to 38 mm.

The SS disc surfaces were cleaned after testing by immersion in 1 M sodium hydroxide solution overnight, sonication in reverse osmosis water at 40 °C for 30 min, followed by drying in air at ambient conditions.

Attempts to characterise the chemical nature of baked lard were made using Fourier transform infrared spectroscopy (FT-IR) and gel permeation chromatography (GPC). FT-IR spectra did not show any marked difference between lard and baked lard (data not presented). GPC testing proved inconclusive, as baked lard did not dissolve in any of the solvents available for testing (including acetone, tetrahydrofuran, chloroform, chlorobenzene and toluene).

2.3. Material rheology

Rheological measurements were conducted using a Bohlin CVO120HR controlled stress rheometer (Malvern Instruments, London, UK) using parallel plates which were either (i) smooth, 20 mm diameter, or (ii) sandblasted, 25 mm diameter, to prevent wall slip. Oscillatory tests were conducted at 20 °C for Vaseline®, VCB paste and lard. Frequency sweeps were performed from 0.01 to 50 Hz with a strain amplitude <1%.

3. Results and discussion

3.1. Material rheology

3.1.1. Honey

Fig. 3 shows that the honey exhibited noticeable shear thinning, with a low shear rate behaviour that is considered pseudo-Newtonian. The non-Newtonian behaviour was attributed to the presence of crystallised sugar particles in the honey. This can be described by the Carreau–Yasuda model:

$$\frac{\eta - \eta_\infty}{\eta_0 - \eta_\infty} = (1 + (\lambda\dot{\gamma})^a)^{(m-1)/a} \quad (4)$$

where η_0 and η_∞ are the low and high shear-rate viscosity, respectively, $\dot{\gamma}$ is the shear rate, λ is a characteristic time constant and parameters a and m describe the behaviour between the low and high-shear rate plateaus. For honey, regression of the experimental data gave $\eta_0 = 13.4$ Pa s, $\eta_\infty = 4$ Pa s, $\lambda = 0.0025$ s, $m = 0$, $a = 1$.

3.1.2. Vaseline® and VCB

The steady shear results in Fig. 4(a) show that both the Vaseline® and VCB pastes exhibit a low shear, high viscosity plateau. Above a critical shear rate, of around 5×10^{-4} s^{-1},

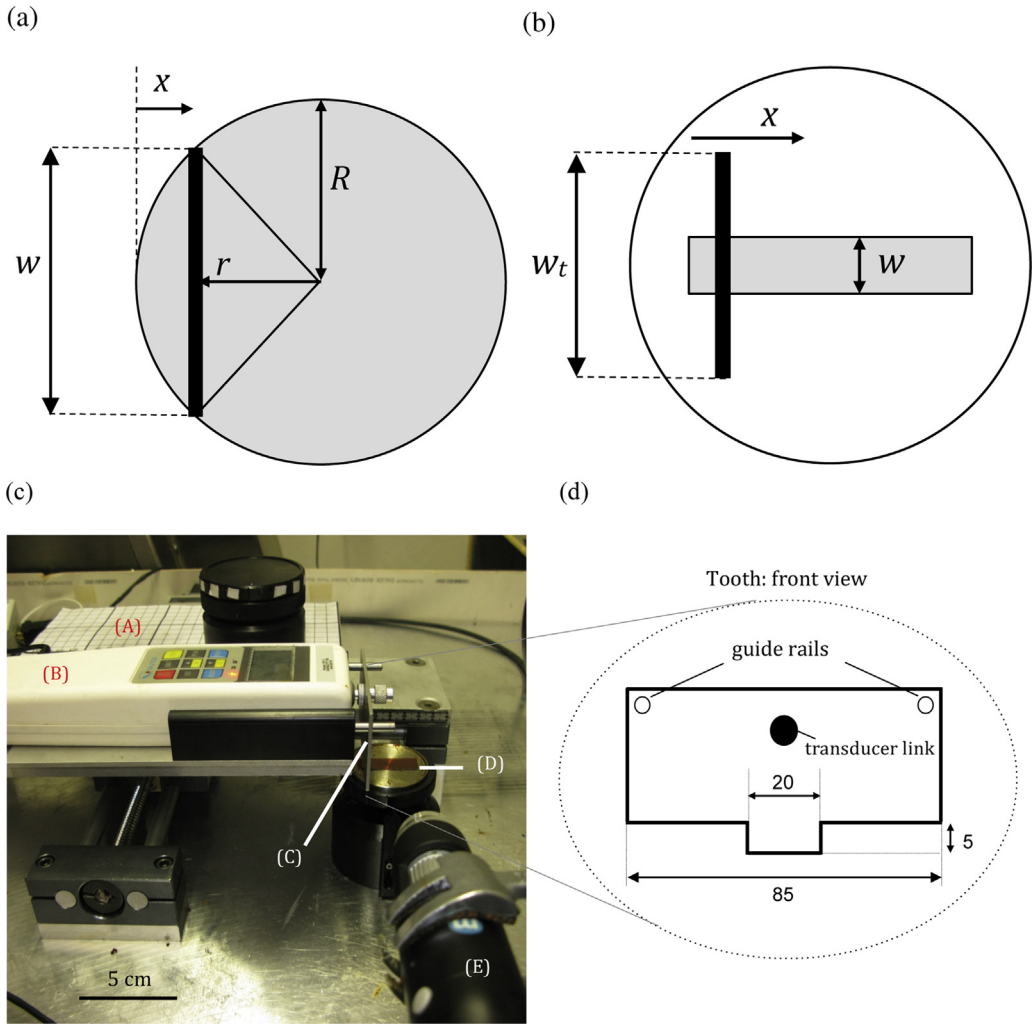

Fig. 2 – (a) Schematic of circular samples, with $w = 2\sqrt{R^2 - (R-x)^2}$. The shaded area denotes the location of the sample. x is the distance scraped through the layer. r is the minimum displacement between the blade and disc centre. r varies between $-R$ and R, such that r/R always lies between -1 and 1. (b) Schematic of rectangular samples. The width of the blade, w_t, is larger than the sample. For the rectangular samples, $w \neq f(x)$. (c) Photograph of the millimanipulation rig showing: (A) motorised x–y table; (B) force transducer; (C) scraper blade held in place with guide rails; (D) adjustable height mount, with baked lard strip; (E) video microscope. (d) Millimanipulation tooth in (b); dimensions in mm.

(shear stress of ~50 Pa) the apparent viscosity decreases strongly with increasing shear rate. The values of the low shear apparent viscosity, of around 10^5 Pa, are similar to those reported for a different Vaseline® material by Chang et al. (2003), as well as some other common food spreads that are not easily cleaned by water rinsing (see (Yang et al., 2014)). When the data are plotted against shear stress, as in Fig. 4(b), they suggest that the material exhibits a critical shear stress of around 50 Pa, above which the material is shear thinning. The effect of slip, giving lower apparent viscosity, is noticeable with smooth tools.

The oscillatory shear data for the Vaseline® based material in Fig. 5 show differences in their small strain behaviour, i.e. before yielding. The viscous modulus, G'', for the Vaseline® is consistently higher than the elastic modulus, G', until higher frequencies, indicating liquid-like behaviour, whereas the VCB moduli values are more similar in magnitude, indicating that a gel-like structure is created by the addition of carbon black particles.

3.1.3. *Lard*

The lard proved to be too stiff for steady shear testing at 20 °C. The oscillatory shear data in Fig. 6, however, show that the lard was predominantly elastic at this temperature, with $G' \sim 15$ kPa, over the frequency range tested. The viscous modulus was ~10 kPa, so some viscoelastic contribution is expected.

3.2. *Millimanipulation data*

3.2.1. *Honey*

Tests with honey employed a 1 mm shear gap. The forces required to deform the honey were small so these tests employed circular shapes and a 60 mm wide blade. Fig. 7(a) shows measured force versus scraped distance for a honey layer of initial thickness 3.5 mm subject to a scrape depth of 2.5 mm. The length of the blade in contact with the film, w, varied with position and the variation is plotted alongside the measured force. The force initially increases as w increases and decreases after x reached the point of maximum width (at $x = R = 31.75$ mm). Separate tests established that compliance in the fittings gave an uncertainty of around ±2 mN in the force measurements.

The force data are plotted as normalised force versus dimensionless scraping distance, r/R, in Fig. 7(b). There is an

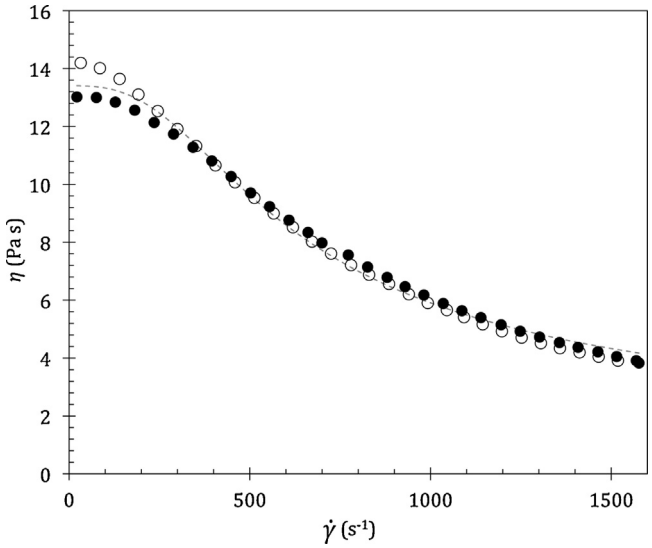

Fig. 3 – Apparent viscosity of honey measured at 20 °C. 1 mm gap, 20 mm radius smooth plates. Solid symbols indicate increasing shear rate, open symbols return ramp (decreasing shear rate). Dashed line shows fit of data to Carreau–Yasuda model, Eq. (4), with parameters $\eta_0 = 13.4$ Pa s, $\eta_\infty = 4$ Pa s, $\lambda = 0.0025$ s, $m = 0$, $a = 1$, $R^2_{fit} = 0.986$.

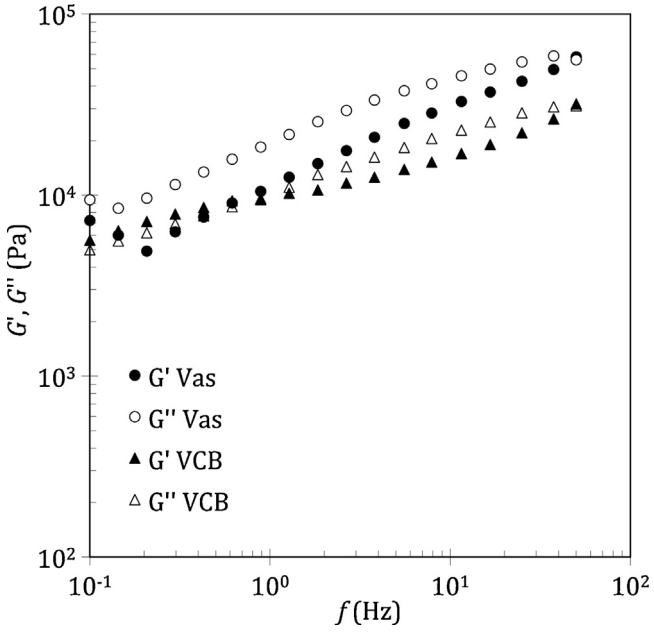

Fig. 5 – Oscillatory testing of Vaseline® (Vas) and Vaseline®-black paste (VCB) at 20 °C. 25 mm diameter, parallel, roughened plates, 1% strain amplitude, 1.5 mm gap.

initial step in F_w over the first few mm of travel, associated with the shear gap being filled, and a steady increase with x until the disc midpoint is reached then decreasing as x increases. The asymmetry evident in Fig. 7(a) is again evident and F_w increases sharply as x approaches and passes $x = 2R$ as w approaches zero. The force profile is not symmetrical about $x = R$, and there is a non-zero force when the blade reaches the edge of the disc ($x = 63.5$ mm).

The linear shear rate in the gap was estimated using:

$$\dot{\gamma} = \frac{V - V_{substrate}}{\delta} \quad (5)$$

where $V_{substrate}$ is the velocity at the substrate. A no-slip boundary condition was assumed, giving $\dot{\gamma} = V/\delta$. The largest shear rate expected under the blade for the velocities in Fig. 7(b), 1–4 mm s^{-1}, is then 4 s^{-1}. At this shear rate, Fig. 3 indicates that the honey is Newtonian with a viscosity of ~14 Pa s.

The contribution of shear, process III, can be estimated by treating the gap under the blade as a one-dimensional slit, so that:

$$F_w^{III} = L\tau_w = L\eta\frac{V}{\delta} \quad (6)$$

where τ_w is the wall shear stress and L, the blade thickness, is 2 mm. For the conditions in Fig. 7(b), the apparent shear stress rates are 1–4 s^{-1} and F_w^{III} = 25–100 mN m^{-1}. These values are all smaller than the initial F_w (measured at $r/R \sim -1$), indicating that F_w is dominated by deformation and displacement.

The F_w profiles in Fig. 7(b) show a proportional dependency on V, which is expected for a Newtonian fluid undergoing

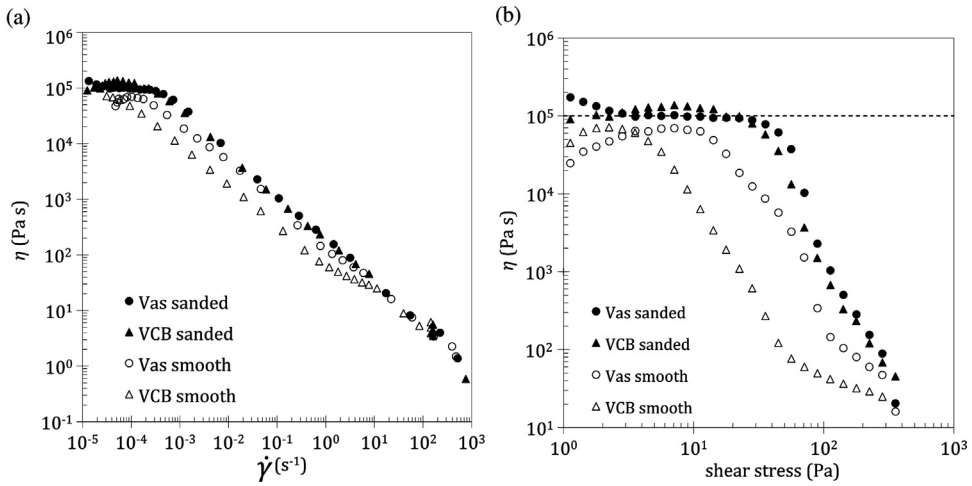

Fig. 4 – Plots of apparent viscosity versus (a) shear rate and (b) shear stress for Vaseline® (labelled 'Vas') and Vaseline®-carbon black (labelled 'VCB') paste at 20 °C. (b) is reproduced from Yang et al. (2014), with permission.

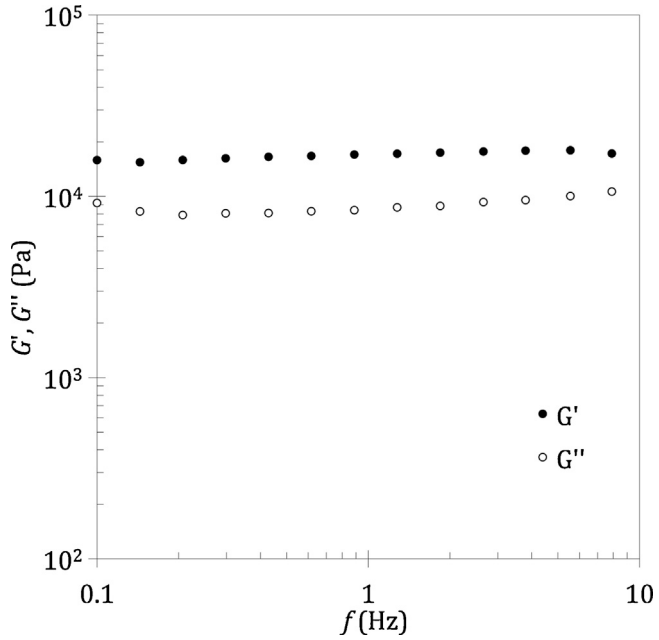

Fig. 6 – Oscillatory testing of lard at 20 °C. Rough parallel plates, 1% strain, 1 mm gap.

shear and deformation in the laminar region. Inspection of the F_w at $r/R = 0$, $F_{w,0}$, showed a linear correlation with V, viz.

$$F_{w,0}(r/R = 0) = 133V + 0.15 \qquad (R^2_{fit} = 0.997) \tag{7}$$

where R^2_{fit} is coefficient of determination.

Video images indicated that the dislodged material accumulated at the front of the blade (as shown in Fig. 1), and beyond the mid-point, i.e. r/R> 0, some dripped off the edge of the disc. The contribution from displacement (process II in Fig. 1) with circular samples is therefore complex and is believed to be responsible for the change in F_w with x. Tests on baked lard were subsequently performed with rectangular strips of material so that the area of sample displaced by the blade is almost constant.

3.2.2. *VCB paste*

The results for removing VCB paste layers, at a scrape depth of 1 mm, in Fig. 8(a) show the increase in f with scrape width observed with honey and a similar asymmetry in the profiles. The forces are noticeably larger, reaching 250 mN compared to the 18 mN observed with honey for scrape depth, $s = 1$ mm, $V = 1$ mm s^{-1}. The measured force is insensitive to the gap height, δ, which varies from 2 to 8 mm in these tests, indicating that F_w^{III} is negligible (estimated as 2 mN m^{-1} using Eq. (6)) and that the device is measuring the cohesive strength of the material.

The normalised profile in Fig. 8(b) shows 3 regions present. In region A, there is a steep initial rise in F_w for $-1 \leq r/R \lesssim -0.85$, to about 2 N m^{-1}. The insensitivity to δ is again evident. The initial rise in A is attributed to some initial creep and compliance in the material.

In region B, the gradual increase in F_w by 1–2 N m^{-1} with displacement is likely due to accumulation of dislodged material in front of the blade. The contribution of hydrostatic stress to F_w, arising from raising the mass of dislodged material, was estimated by $\rho g V_{displace}$ as $\sim 5 \times 10^{-5}$ N (where $V_{displace}$ is the volume of displaced material). Process II, was not therefore considered to affect millimanipulation data. In region C, F_w rises markedly, as w approaches zero. This was also observed with honey (see Fig. 7(b)) and these data are discarded.

Tests on 12 mm wide rectangular VCB samples are shown in Fig. 9. The force values in Fig. 9(a) are lower than the disc tests (Fig. 8), as the width of the tooth is generally smaller than the chord in contact with the sample in the disc tests. The simpler deformation zone ahead of the blade may be the reason why there is no gradual rise in F_w. Region C in Fig. 8(b) is not evident. As with the disc tests, initial sample thickness does not affect the results and the magnitudes of F_w (~2–3 N m^{-1}) are similar.

Fig. 10 shows the effect of scrape depth, where layers of different initial thickness were scraped to a common residual thickness, of 5 mm. The apparent shear rate under the blade in these cases is 0.2 s^{-1} and the F_w^{III} contributions estimated from Eq. (6) is around 0.4 N m^{-1}. The individual profiles do not

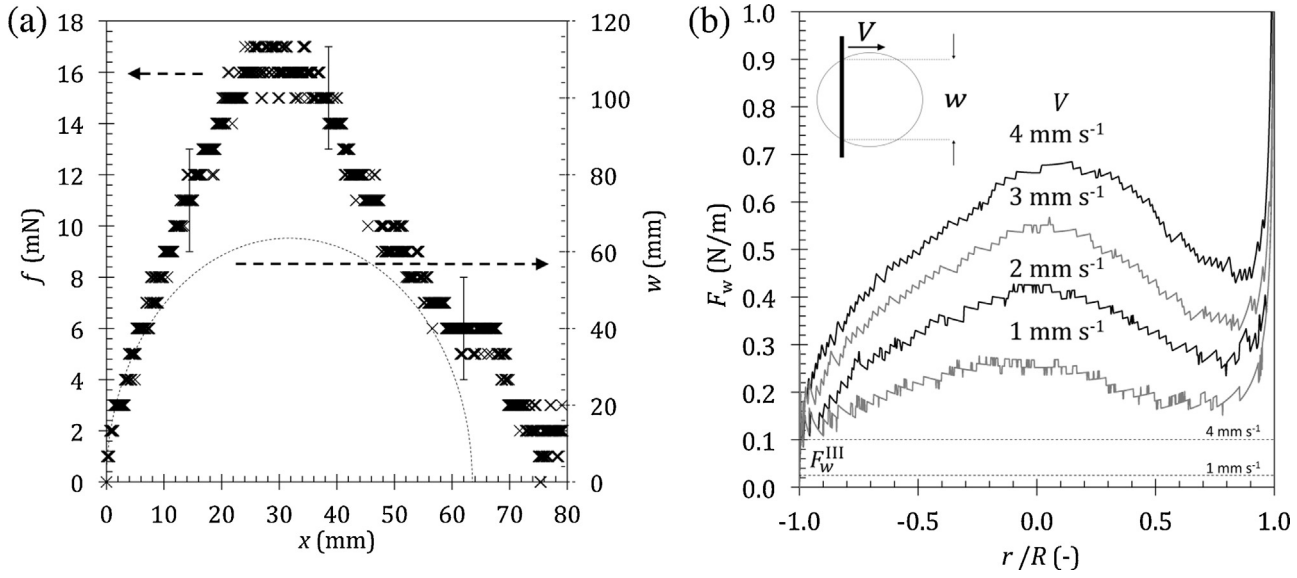

Fig. 7 – Millimanipulation of honey on 63.5 mm diameter circular SS discs at 20 °C. $\delta_o = 3.5$ mm, $s = 2.5$ mm, $R = 31.75$ mm. (a) Force, f, and blade contact length, w, for $V = 1$ mm s^{-1}. Error bars on selected points show measurement uncertainty. Gaps between data points are due to the limits of the force transducer resolution. (b) Effect of velocity on F_w, with normalised scrape force versus distance. The horizontal dashed lines indicate estimated values of F_w^{III} from Eq. (6).

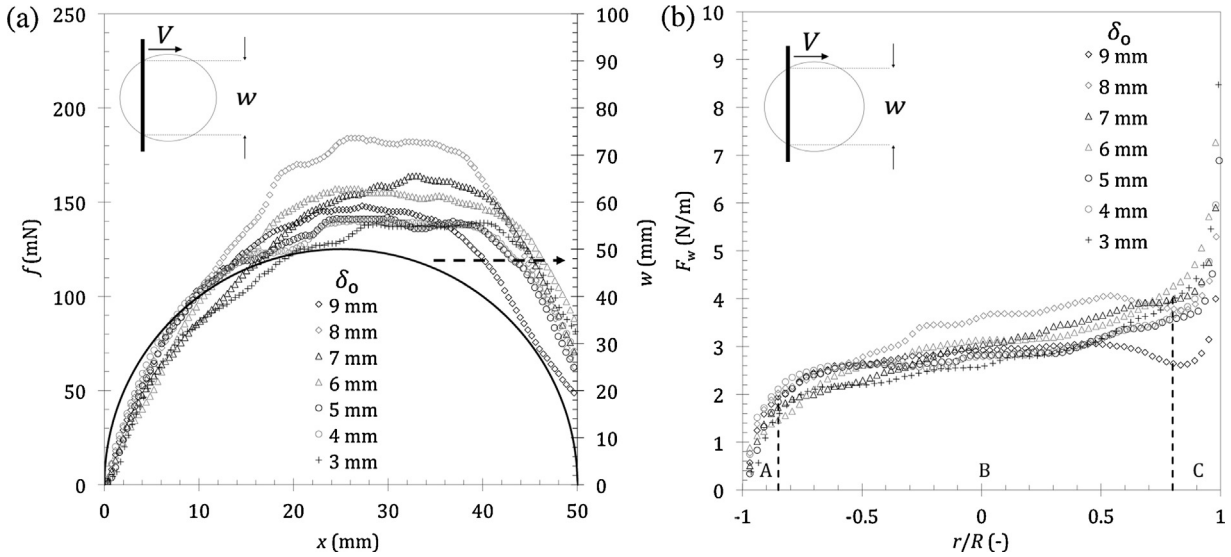

Fig. 8 – Removal of VCB paste from 50 mm diameter discs. $V = 1\,mm\,s^{-1}$, $s = 1\,mm$, $R = 25\,mm$, 20 °C. (a) raw data, including blade contact length, w, displayed with the solid line. (b) normalised force versus normalised radial distance. Legend entries indicate initial sample thickness δ_o.

exhibit the trends in Fig. 8, except for $s = 1\,mm$. For $s = 2\,mm$ and 4 mm, there is a rise in F_w until $r/R \sim -0.5$ after which point there is a gradual decrease in F_w. In addition the F_w values in region B do not increase proportionately with s, which would be expected if F_w^I and F_w^{II} were related to the volume of material deformed and displaced. The deformation of the VCB material is complex and is the subject of ongoing investigation.

3.2.3. *Lard*

The profiles obtained for scraping circular lard samples in Fig. 11(a) show similar features to the VCB paste in Fig. 8(b). Samples were also prepared as rectangular strips. F_w values for the rectangular sections in Fig. 11(b) were, in general, lower that on the circular disc. The reason for the differences is not currently understood. There is also more variation between samples on the discs. The trends observed remain the same between testing on the rectangular section and discs; in particular, scrape speed did not affect F_w.

The measured forces for lard are about 3 times larger than the VCB paste. There is, however, no simple relationship between f and the rheometry data. The scraping speed has no effect on F_w, indicating that F_w^{III} is small. For soft solids that fail in a cohesive manner, a flat surface is left behind (see schematic in Fig. 1(a)). Therefore, by returning the blade over the scraped sample, separate measurements of F_w^{III} can be made. For lard, these measurements confirmed that $F_w^{III} < 0.3\,mN$. The insensitivity to V indicates that the deformation is primarily due to elastic and plastic components.

3.2.4. *Baked lard*

The behaviour observed for baked lard different markedly from lard. The results for baked lard reported in Fig. 12 were obtained with 12 mm wide strip samples tested using the tooth tool (Fig. 2(b)–(d)). Fig. 12 presents a typical plot of F_w versus time, rather than displacement, obtained for a sample

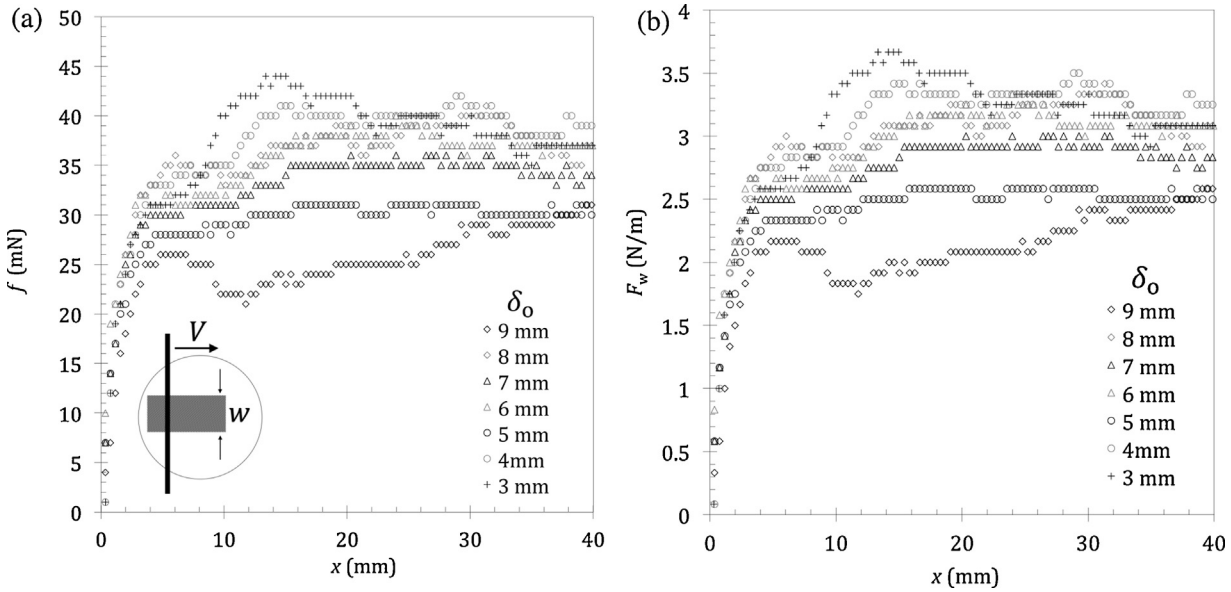

Fig. 9 – Removal of VCB paste from 12 mm wide rectangular sections. $V = 1\,mm\,s^{-1}$, $s = 1\,mm$, 20 °C. (a) Scrape profiles. (b) Normalised force versus x. Legend entries indicate initial sample thickness δ_o.

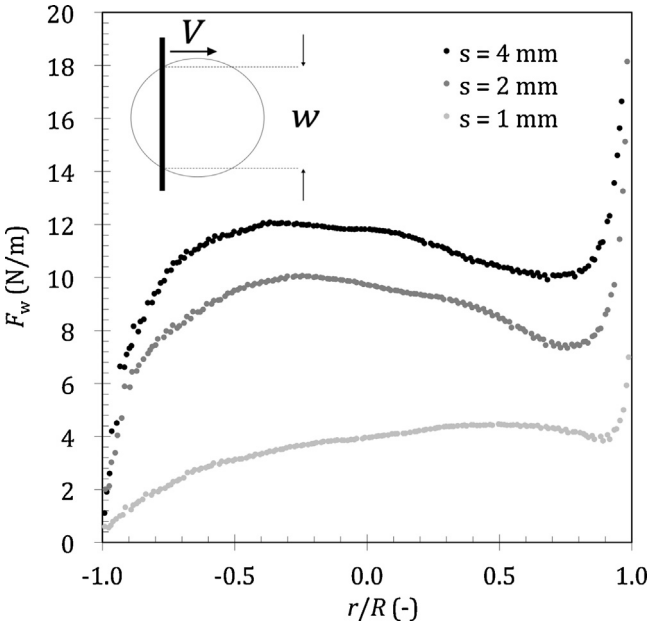

Fig. 10 – Effect of scrape depth, s, on F_w for VCB paste on circular discs. 20 °C, V = 1 mm s^{-1}, δ = 5 mm, R = 25 mm, δ_o varies (=5 mm + s).

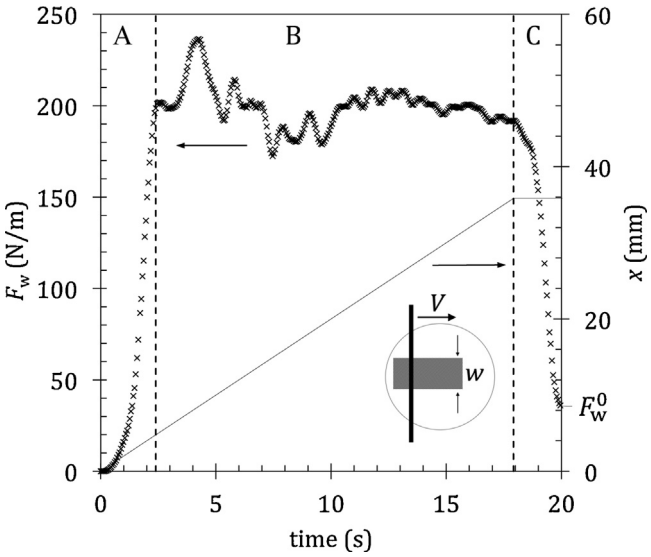

Fig. 12 – Plot of F_w and displacement, x, versus time for lard baked for 4 h at 250 °C. Test conditions: T = 20 °C, V = 2 mm s^{-1}, δ_o = 0.6 mm, s = 0.4 mm. F_w^0 marked on as the residual force remaining after scraping.

of protein-free lard baked at 250 °C for 4 h and scraped at V = 2.0 mm s^{-1}. The blade moved through the sample, leaving a 0.2 mm residual film, until x = 38 mm, at which point it halted (at t = 19 s). As before, three regions are evident. In the initial region, marked A, there is a steep, initial rise. The point at which F_w begins to rise is set as the origin. This behaviour is attributed to compliance and initial creep (elasticity) in the material. The existence of creep was confirmed by halting the motion of the blade during a traverse. The force decayed to a small value, F_w^0, in an exponential manner. Videos confirmed that this decay was not due to movement of the soil, indicating visco-elastic behaviour and consistent with the material developing stronger and new cohesive interactions as a results of oxidative polymerisation (Wilson and Watkinson, 1996).

In region B, F_w fluctuates around an average value, denoted $\overline{F_w}$. This is interpreted as arising from steady shear and yielding within the material, and the magnitude of $\overline{F_w}$ is taken here to represent the cohesive strength of the layer. The fluctuations arise due to brittle fracture and ductile deformation of this sample (i.e. cracking and creation of new surfaces). Samples cooked at lower temperatures and shorter times tended to exhibit ductile yielding and gave more uniform F_w profiles, as well as even residual layers.

In region C, the blade is stationary, near the end of the sample. The blade is still in contact with the layer and F_w decays with time. This was also observed in the creep tests referred to above. It is noticeable that F_w does not decay to zero, but approaches a residual value of around 37 N m^{-1}, suggesting a plastic component to the deformation.

The time dependent decay in F_w was investigated by halting a traverse before approaching the end of the sample, as shown in Fig. 13(a). F_w had reached a steady value of ~115 N m^{-1} before motion was halted at ~2.5 s. The force decays to a measurable residual F_w^0, of around 20 N m^{-1}. The

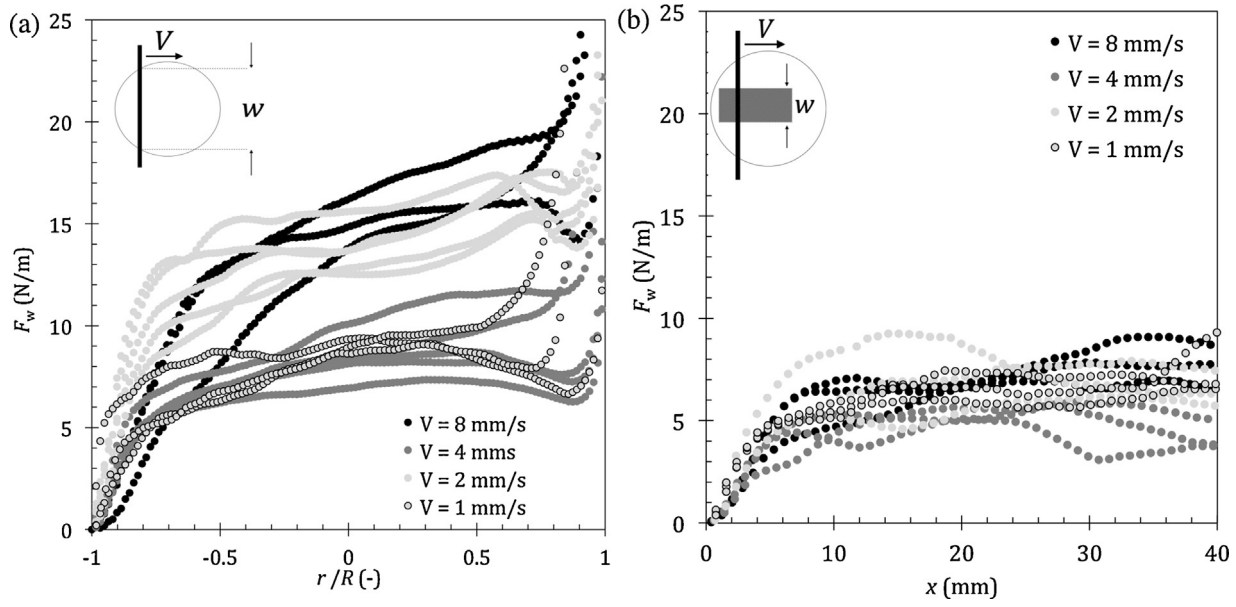

Fig. 11 – Effect of V on F_w for (a) circular (R = 25 mm) and (b) rectangular strip lard samples. 20 °C, δ_o = 6.7 mm, s = 1 mm.

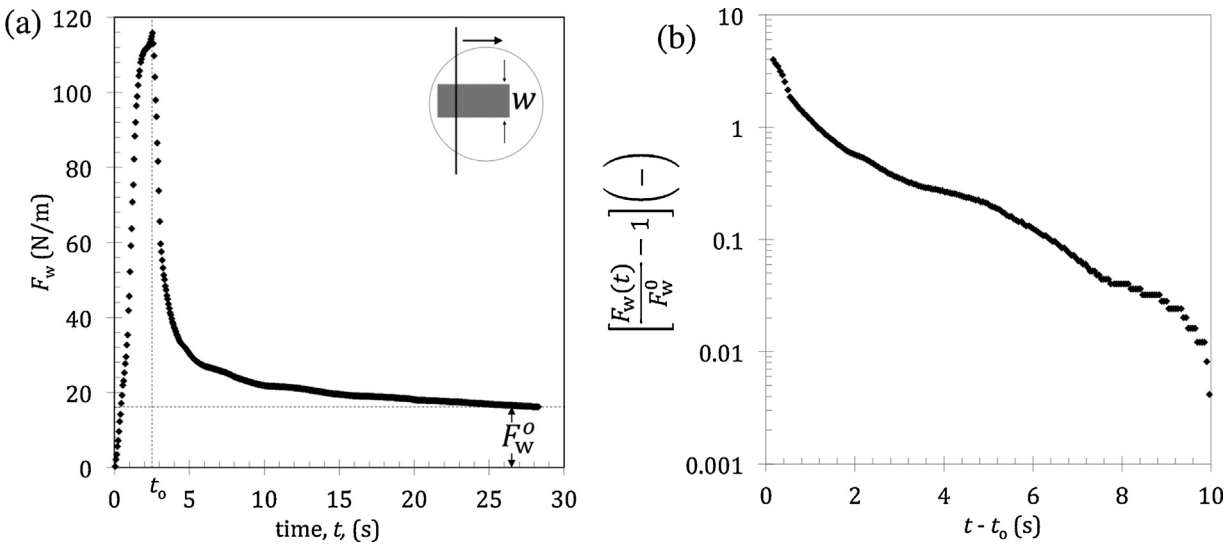

Fig. 13 – Decay in measured force after scraping is halted at time t_0. Strip sample of lard baked for 4 h at 250 °C. The blade is moved 5 mm into a 40 mm long sample at 2 mm s^{-1} then stopped at $t_0 = 2.5$ s. 20 °C, $\delta_o = 0.6$ mm, $s = 0.4$ mm. (a) $F_w - t$ profile, with residual force F_w^o. (b) Data in (a) plotted in the form of exponential decay.

transient data are plotted in the form of an exponential decay model in Fig. 13(b) and exhibit a roughly linear trend on log-linear axes. This suggests that the stress relaxation could be approximated by a single-element Maxwell model, but a multi-mode model may be more appropriate.

3.2.4.1. *Types of removal.* There are three types of removal observed for these layers. If the layers fail adhesively, a clean substrate is left behind after scraping (see Fig. 14(a)). Adhesive strength would be assessed by either (i) scraping off close to the disc surface (i.e. setting $\delta \sim 0$) or (ii) if the adhesive strength is sufficiently lower than the cohesive strength such that the soil–substrate bond yields before soil–soil bonds do. If they fail cohesively, a residual layer will remain after scraping. For the harder, baked lard layers, this will leave a jagged, uneven wake, of varying thickness (see Fig. 14(b)). If the layer fails both adhesively and cohesively, a mixture of the patterns in Fig. 14(a) and (b) is observed.

3.2.4.2. *Effect of testing conditions.* Fig. 15 shows the effect of scrape velocity on the removal behaviour of polymerised lard layers prepared by baking at 250 °C for 4 h. Each datum represents a separate experiment and there is noticeable variation between tests, which is partly due to the extent of polymerisation not being controllable with this material. The variation between samples is significantly greater than the fluctuation in F_w for individual samples, marked by the error bars.

There is noticeable scatter at the lowest scrape speed ($V = 0.5$ mm s^{-1}) which is accompanied by a mixture of cohesive and adhesive failure. At higher speeds removal is dominated by the latter mode. The weak dependency on V confirms that the materials exhibit plastic behaviour. The

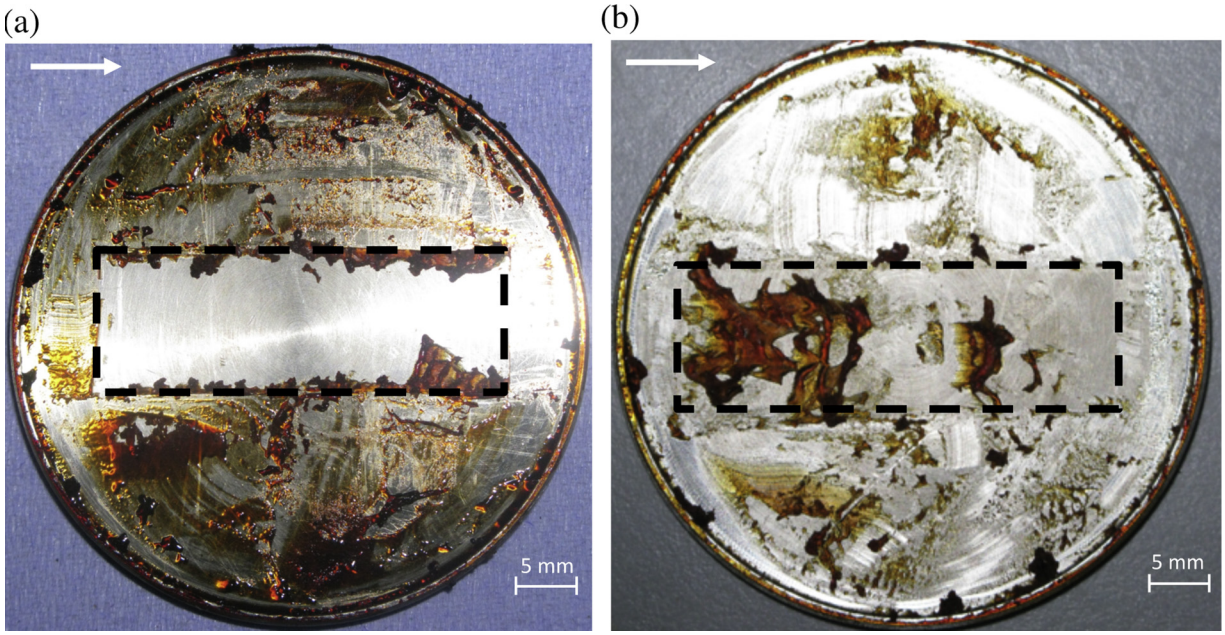

Fig. 14 – Photographs of wake region after millimanipulation scraping of lard baked at 250 °C. $V = 2$ mm s^{-1}, $\delta_o = 0.6$ mm, $s = 0.4$ mm. Arrow indicates direction of scraping. Dashed lines indicate regions where the sample was scraped away. (a) Adhesive failure and (b) cohesive failure.

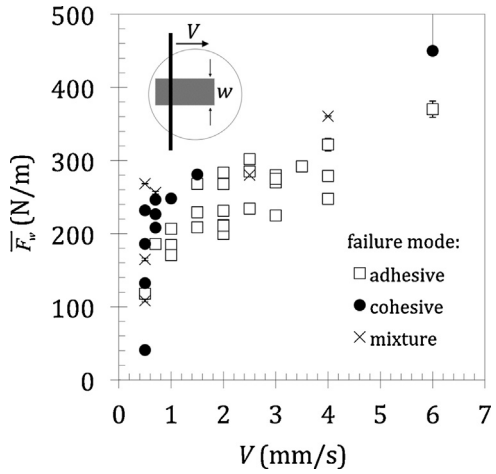

Fig. 15 – Effect of scrape speed on $\overline{F_w}$ for lard baked for 4 h at 250 °C. Solid circles – cohesive failure; open squares – adhesive failure. Crosses indicate a mixture of cohesive and adhesive failure. Test conditions = 20 °C, δ_o = 0.6 mm, s = 0.4 mm. Bars represent 95% confidence intervals. For most data points, the symbol is larger than error bar.

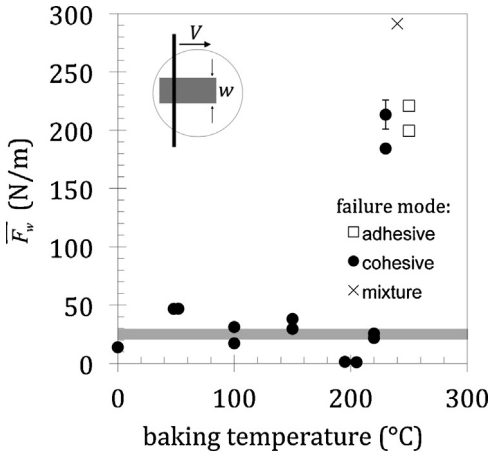

Fig. 16 – Effect of baking temperature on $\overline{F_w}$ for lard baked for 5 h. 40 mm long strips, δ_o = 0.6 mm, s = 0.4 mm, V = 2 mm s^{-1}. Solid circles – cohesive failure; open squares – adhesive failure. Crosses indicate a mixture of cohesive and adhesive failure. Shaded region denotes values of $\overline{F_w}$ observed for unbaked lard in Fig. 11. Some data points have been offset on the temperature axis for clarity. Error bars represent 95% confidence intervals.

prevalence of adhesive failure at higher velocities suggests that the cohesive strength is velocity dependent, and as the forces induced by the blade increase, the adhesive bonds – which are not determined by V – rupture.

The effect of scrape depth on millimanipulation measurements was examined for samples with δ_o = 0.6 mm. The sample height could be adjusted manually at 0.1 mm increments. For small clearances (≤0.30 mm), the blade compressed the lard layer and consequently bounced over the top of the sample. At a scrape depth of 0.5 mm (i.e. a clearance of 0.1 mm), the force measured by the transducer exceeded the limit on the device. This left a scrape depth of 0.4 mm as the only sample height under which millimanipulation measurements could be made for these, harder, layers with this version of the device.

3.2.4.3. *Effect of baking conditions.* Fig. 16 shows the effect of baking temperature on lard baked for 5 h. Baking at or below 220 °C gave a soft solid layer which exhibited cohesive fracture, with the dislodged material adhering to and climbing up the blade. The layers remained semi-solid and wax-like even if baked for several days. The residual layers had a smooth surface and a rescan of this layer gave an estimate of F_w^{III}. This force was consistently much smaller (2–3%) of the $\overline{F_w}$ values in Fig. 16, indicating that shear in the gap was not significant.

The layers harden noticeably above 225 °C, with $\overline{F_w}$ reaching 200–300 N m^{-1}. These layers were solid when removed from the oven and tended to coke (i.e. burn) before melting when heated in air. Separate DSC tests (data not presented here) confirm that the melting temperature of the baked lard exceeded 300 °C. The layers fractured unevenly, at weak points within the soil, or at the soil–substrate interface. At 240 °C the strength of the adhesive and cohesive bonds was comparable and the failure mode observed was mixed. At 250 °C, the layers tended to fail adhesively, where the material cohesive strength was stronger than the adhesion to the substrate and the layer peeled off.

The increase in strength is associated with oxidative polymerisation (autoxidation). This is an autocatalytic process and requires free radical initiation, which is hindered by the presence of an antioxidant, butylated hydroxytoluene (BHT) present in the lard to inhibit rancidification. Increasing the baking temperature increases the rate of BHT consumption, reducing the induction period before autoxidation starts in earnest. This is reflected in the results for different baking times in Fig. 17.

3.2.5. *Baked lard + ovalbumin*

As many food soils contain both fats and proteins (as well as other species), the influence of protein on the lard layers was investigated. Lard–ovalbumin mixtures were baked at 250 °C for 3, 4 and 5 h, crossing the hardening transition observed with lard at this temperature (Figs. 16 and 17). The results are summarised in Fig. 18. For all mixtures, the force required to deform the material increases with baking time.

When baking for 3 h, addition of ovalbumin suppresses autoxidation, so that the layers do not polymerise and remain as soft semi-solid soils. After 4 h, $\overline{F_w}$ for the 1 wt% ovalbumin is ~100 N m^{-1} and the layer exhibits predominantly cohesive

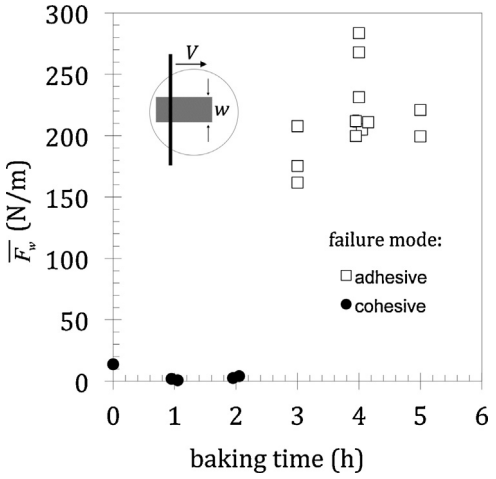

Fig. 17 – Effect of baking time on $\overline{F_w}$ for lard baked at 250 °C. Some data points have been offset on the (baking) time axis for clarity. Test conditions; 20 °C, δ_o = 0.6 mm, s = 0.4 mm, V = 2 mm s^{-1}. Error bars represent 95% confidence intervals.

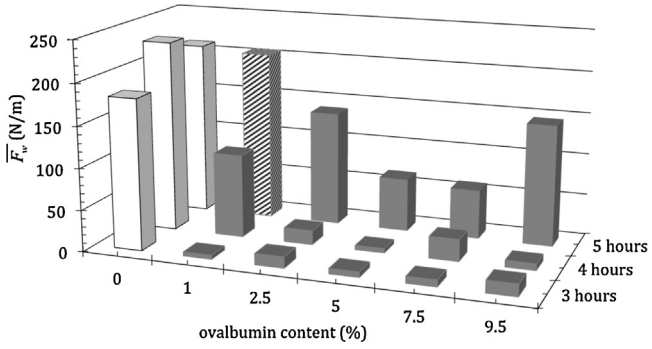

Fig. 18 – Effect of ovalbumin content on $\overline{F_w}$ for lard mixtures baked for 3–5 h at 250 °C. White and grey blocks denote sets of tests where all samples have failed adhesively or cohesively, respectively. The hatched block marks where a mixture of adhesive and cohesive failure was observed. Testing conditions = 20 °C, δ_o = 0.6 mm, s = 0.4 mm, V = 2 mm s^{-1}.

failure, which is associated with unpolymerised layers. In contrast, the lard-only layers exhibit adhesive failure, with $\overline{F_w}$~220 N m^{-1}. Mixtures with higher ovalbumin content are still soft semi-solids, all of which fail cohesively.

Baking for 5 h creates stronger samples for all protein concentrations. The 1 wt% protein layers give $\overline{F_w}$ values similar to protein-free lard and, like the lard, tend to exhibit adhesive failure, indicating that the cohesive strength of the material exceeds the interactions with the substrate. There is a noticeable minimum in $\overline{F_w}$ with increasing protein content. As the ovalbumin content is increased, up to 7.5 wt%, the presence of protein tends to reduce the strength of the layer. All these layers exhibit cohesive failure, suggesting that polymerisation occurs but at lower rates in the presence of more protein. At 9.5 wt% ovalbumin, however, there is a significant increase in $\overline{F_w}$ and the data are widely scattered. For these layers, several black specks (with a radius ~0.1 mm) were visible in the layer. This is attributed to agglomeration of proteins and reaction of these agglomerates to form a secondary structure.

These results confirm that the nature and properties of polymerised food fat soils are sensitive to their composition and thermal history. A single model material is unlikely to be able to exhibit the range of soiling layers encountered in practice, so careful consideration is required in the selection of test soils and application of the results to real soils. Likewise, the chemical composition of real fat soils is likely to vary widely in terms of protein nature loading, levels and type of unsaturated fat and antioxidant content. The millimanipulation device does, nevertheless, offer a method for characterising the nature of the soils and quantifying their removal behaviour. The effect of detergents and cleaning solutions on weakening these layers and/or promoting adhesive removal can be investigated using relatively small samples and a range of substrates.

4. Conclusions

A novel millimanipulation device has been developed to test the deformation behaviour and quantify cohesive and adhesive strengths of soft solid fouling layers on lab scale surfaces. A viscous liquid, honey, and a viscoplastic material, a Vaseline® carbon-black paste, were used to assess the effect of layer rheology on deformation behaviour.

Lard was used a model food soil. Unbaked lard exhibited viscoplastic behaviour and was removed by cohesive failure. Baking the lard in air had no effect until autoxidative polymerisation occurred, which was marked by an increase in cohesive strength from ~25 N m^{-1} to over 200 N m^{-1}. Extended baking promoted adhesive failure (rupture at the substrate), indicating that the interactions within the polymerised material were stronger than those with the SS 316 substrate. Increasing scrape velocity promoted adhesive failure, which is likely due to viscoelastic contributions.

Addition of ovalbumin to the lard tended to delay the onset of polymerisation. Higher protein contents results in additional protein-protein interactions and confirmed the complexity of these food soils.

Acknowledgments

An EPSRC studentship for AA is gratefully acknowledged, as it project support and a summer studentship for JP from Proctor & Gamble.

References

Akhtar, N., Bowen, J., Asteriadou, K., Robbins, P.T., Zhang, Z., Fryer, P.J., 2010. Matching the nano- to the meso-scale: measuring deposit–surface interactions with atomic force microscopy and micromanipulation. Food Bioprod. Process. 88, 341–348.

Bakker, D.P., Van Der Plaats, A., Verkerke, G.J., Busscher, H.J., Van Der Mei, H.C., 2003. Comparison of velocity profiles for different flow chamber designs used in studies of microbial adhesion to surfaces. Appl. Environ. Microbiol. 69, 6280–6287.

Bayoudh, S., Ponsonnet, L., Ouada, H.B., Bakhrouf, A., Othmane, A., 2005. Bacterial detachment from hydrophilic and hydrophobic surfaces using a microjet impingement. Colloids Surf. A: Physicochem. Eng. Aspects 266, 160–167.

Chang, G.S., Koo, J.S., Song, K.W., 2003. Wall slip of vaseline in steady shear rheometry. Korea–Aust. Rheol. J. 15, 55–61.

Chew, J.M., Cardoso, S.S.S., Paterson, W.R., Wilson, D.I., 2004. CFD studies of dynamic gauging. Chem. Eng. Sci. 59, 3381–3398.

Detry, J.G., Rouxhet, P.G., Boulang-Petermann, L., Deroanne, C., Sindic, M., 2007. Cleanability assessment of model solid surfaces with a radial-flow cell. Colloids Surf. A: Physicochem. Eng. Aspects 302, 540–548.

Garca, A.J., Ducheyne, P., Boettiger, D., 1997. Quantification of cell adhesion using a spinning disc device and application to surface-reactive materials. Biomaterials 18, 1091–1098.

Garrett, T.R., Bhakoo, M., Zhang, Z., 2008. Bacterial adhesion and biofilms on surfaces. Prog. Nat. Sci. 18, 1049–1056.

Liu, W., Aziz, N., Zhang, Z., Fryer, P., 2007. Quantification of the cleaning of egg albumin deposits using micromanipulation and direct observation techniques. J. Food Eng. 78, 217–224.

Liu, W., Christian, G., Zhang, Z., Fryer, P., 2002. Development and use of a micromanipulation technique for measuring the force required to disrupt and remove fouling deposits. Food Bioprod. Process. 80, 286–291.

Liu, W., Christian, G., Zhang, Z., Fryer, P., 2006a. Direct measurement of the force required to disrupt and remove fouling deposits of whey protein concentrate. Int. Dairy J. 16, 164–172.

Liu, W., Fryer, P., Zhang, Z., Zhao, Q., Liu, Y., 2006b. Identification of cohesive and adhesive effects in the cleaning of food fouling deposits. Innov. Food Sci. Emerg. Technol. 7, 263–269.

Liu, W., Zhang, Z., Fryer, P., 2006. Identification and modelling of different removal modes in the cleaning of a model food deposit. Chem. Eng. Sci. 61, 7528–7534.

Wilson, D.I., Watkinson, A.P., 1996. A study of autoxidation reaction fouling in heat exchangers. Can. J. Chem. Eng. 74, 236–246.

Yang, Q., Ali, A., Shi, L., Wilson, D.I., 2014. Zero discharge fluid dynamic gauging for studying the thickness of soft solid layers. J. Food Eng. 127, 24–33.

Yap, S.F., Adams, M., Seville, J., Zhang, Z., 2006. Understanding the mechanical properties of single micro-particles and their compaction behaviour. China Particuol. 4, 35–40.

Zhang, Z., Al-Rubeai, M., Thomas, C., 1992. Mechanical properties of hybridoma cells in batch culture. Biotechnol. Lett. 14, 11–16.

Zhang, Z., Ferenczi, M.A., Lush, A.C., Thomas, C.R., 1991. A novel micromanipulation technique for measuring the bursting strength of single mammalian cells. Appl. Microbiol. Biotechnol. 36, 208–210.

Zorita, S., Niquet, C., Bonhoure, J.P., Robert, N., Tessier, F.J., 2010. Optimisation of a model food mixture using response surface methodology to evaluate the anti-adhesive properties of cooking materials. Int. J. Food Sci. Technol. 45, 2494–2501.